

Article

Crystalline AlN Interfacial Layer on GaN Using Plasma-Enhanced Atomic Layer Deposition

Il-Hwan Hwang ¹, Myoung-Jin Kang ¹ , Ho-Young Cha ^{2,*} and Kwang-Seok Seo ^{1,*}

¹ Department of Electrical and Computer Engineering, Inter-University Semiconductor Research Center, Seoul National University, Seoul 151-744, Korea; hih0705@gmail.com (I.-H.H.); mj kang5@snu.ac.kr (M.-J.K.)

² School of Electronic and Electrical Engineering, Hongik University, Seoul 121-791, Korea

* Correspondence: hcha@hongik.ac.kr (H.-Y.C.); ksseo@snu.ac.kr (K.-S.S.); Tel.: +82-10-4151-7275 (K.-S.S.)

Abstract: In this study, we report on the deposition of a highly crystalline AlN interfacial layer on GaN at 330 °C via plasma-enhanced atomic layer deposition (PEALD). Trimethylaluminum (TMA) and NH₃ plasma were used as the Al and N precursors, respectively. The crystallinity and mass density of AlN were examined using X-ray diffraction (XRD) and X-ray reflectivity (XRR) measurements, respectively, and the chemical bonding states and atomic concentrations of the AlN were determined by X-ray photoelectron spectroscopy (XPS). The AlN/n-GaN interface characteristics were analyzed using TOF-SIMS and STEM, and the electrical characteristics of the AlN were evaluated using metal-insulator-semiconductor (MIS) capacitors. The PEALD process exhibited high linearity between the AlN thickness and the number of cycles without any incubation period, as well as a low carbon impurity of less than 1% and high crystal quality even at a low deposition temperature of 330 °C. Moreover, the GaN surface oxidation was successfully suppressed by the AlN interfacial layer. Furthermore, enhanced electrical characteristics were achieved by the MIS capacitor with AlN compared to those achieved without AlN.



Citation: Hwang, I.-H.; Kang, M.-J.; Cha, H.-Y.; Seo, K.-S. Crystalline AlN Interfacial Layer on GaN Using Plasma-Enhanced Atomic Layer Deposition. *Crystals* **2021**, *11*, 405. <https://doi.org/10.3390/cryst11040405>

Academic Editor: Alberto Girlando

Received: 25 March 2021

Accepted: 8 April 2021

Published: 10 April 2021

Publisher's Note: MDPI stays neutral with regard to jurisdictional claims in published maps and institutional affiliations.



Copyright: © 2021 by the authors. Licensee MDPI, Basel, Switzerland. This article is an open access article distributed under the terms and conditions of the Creative Commons Attribution (CC BY) license (<https://creativecommons.org/licenses/by/4.0/>).

Keywords: GaN; AlN; AlHfON; ALD; interfacial layer; MIS capacitor

1. Introduction

GaN-based metal-insulator-semiconductor field-effect transistors (MIS-FETs) require a high positive gate voltage for power switching applications. However, this can cause electrons in the two-dimensional electron gas (2DEG) channel to enter the high-density trap states at the dielectrics/(Al)GaN interface, thereby resulting in threshold voltage instability in these devices [1–3]. Therefore, several gate dielectrics, such as SiO₂ [4,5], HfSiO [6,7], SiON [8,9], ZrO₂ [10,11], Al₂O₃ [12,13], AlON [14,15], and HfO₂ [16,17], have been proposed for use as the gate dielectrics of MIS-FETs to improve the dielectric/(Al)GaN interface characteristics. However, some studies have indicated that trap states can be attributed to the poor-quality native oxide (GaO_x) between the dielectric/III–V interface formed during the gate oxide deposition process [18,19]. Gate oxides deposited via thermal atomic layer deposition (ALD) using water as an oxidizing agent have been shown to reduce the interfacial oxide between the dielectric/GaN because of their weaker oxidability compared to O₃ [20]. Our group also reported on the atomic layer deposition (ALD) of HfO₂ using isopropyl alcohol (IPA) as an oxidant during the process, thereby efficiently reducing surface oxidation compared to O₃ [21]. Surface oxidation can also be reduced using nitride-based dielectrics such as Si₃N₄ and AlN. Given that oxidants that suppress surface oxidation are not used in these processes, surface traps and current collapses are reduced, resulting in reliable device performance [22,23]. In particular, AlN has a smaller lattice mismatch between (Al)GaN and AlN [24] compared to that between (Al)GaN and SiN_x, and AlN serves as a good candidate for interfacial layers in GaN-based MIS devices. However, only a few studies have investigated AlN interfacial layers.

In this study, we developed and optimized AlN as an interfacial layer that suppresses the formation of poor-quality oxides. AlN was deposited via plasma-enhanced atomic layer deposition (PEALD) as this approach facilitates better thickness uniformity, film quality, thickness control, and lower impurity concentration than other deposition techniques [25–27]. The material characteristics of AlN were evaluated using X-ray diffraction (XRD), X-ray reflectivity (XRR), scanning transmission electron microscopy (STEM), secondary ion mass spectrometry (SIMS), and X-ray photoelectron spectroscopy (XPS). The leakage current density (J)–effective electric field (E_{eff}) and the capacitance (C)–voltage (V) characteristics of AlN/AlON/AlHfON on GaN were compared with those of AlON/AlHfON on n-GaN.

2. Experiments

ALD AlN deposition was performed in a PEALD system (CN1, Hwaseong-si, Korea) with two chambers: a load-lock and a transfer chamber. This system has showerhead injectors and can accommodate 6-inch wafers. The showerhead was capacitively coupled with an RF of 27.12 MHz and the chuck was grounded. The distance between the showerhead and the chuck was 35 mm. A schematic of the PEALD system is shown in Figure 1.

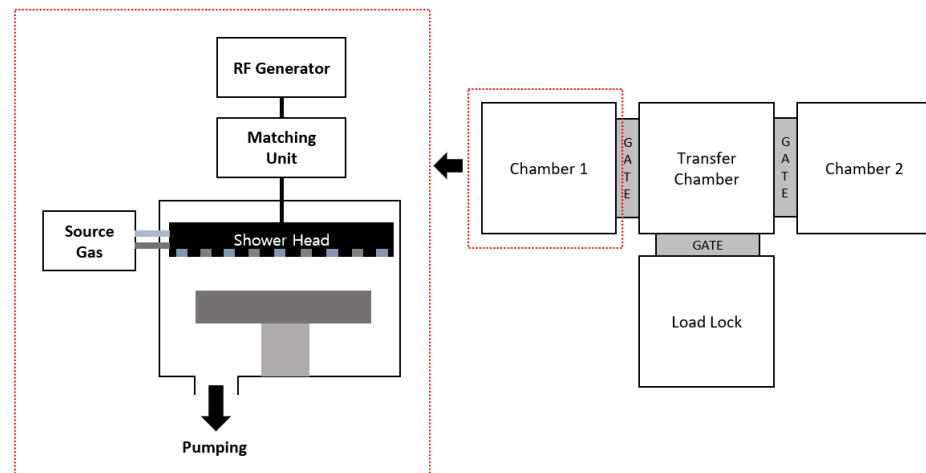


Figure 1. Schematic of plasma-enhanced atomic layer deposition (PEALD) system used for the experiments.

PEALD AlN deposition was performed on n-type Si (111) using trimethylaluminum (TMA) and NH_3 gas as the Al and N precursors, respectively. The temperatures of the gas lines and TMA precursor were 90°C and 5°C , respectively, and the deposition temperature of AlN was 330°C . The temperatures of the upper lid and chamber wall were maintained at 150°C to reduce impurities such as carbon and oxygen in the dielectric layer. Purging was performed using N_2 gas after the TMA precursor injection and NH_3 plasma step, followed by the NH_3 gas stabilization step. The NH_3 plasma and purge step pressures were 120 and 500 mTorr, respectively.

MIS capacitors using n-GaN wafers were fabricated to investigate the electrical properties of AlN on n-GaN. The epitaxial layers consisted of a 300 nm n-GaN layer with a Si doping concentration of $2.5 \times 10^{17} \text{ cm}^{-3}$, 700 nm n-type GaN layer, 700 nm n-GaN layer with a $2\text{--}3 \times 10^{18} \text{ cm}^{-3}$ Si doping concentration, and 3900 nm GaN buffer layer grown on an Si substrate. The effect of NH_3 plasma power on the electrical characteristics of AlN was determined by fabricating MIS capacitors with different plasma powers of 30, 50, and 100 W. Ex situ and in situ treatments were conducted before the AlN deposition. The ex situ treatment included SPM and diluted HF (10:1) to remove organic contaminants and native oxides on the GaN surface. The in situ treatment included TMA pulsing (10 times with a duration of 0.2 s) and NH_3 thermal treatment for 5 min; these two treatments were conducted to remove oxides and for surface nitridation, respectively. After AlN deposition,

postdeposition annealing (PDA) was conducted at 500 °C for 10 min in an ambient N₂ atmosphere. Following ohmic patterning and ohmic recess, ohmic contacts were formed with Ti/Al (40/200 nm) metallization. The ohmic contact formation was annealed at 500 °C under an ambient N₂ atmosphere for 1 min. Finally, an Ni/Au (40/130 nm) metal electrode was deposited via e-gun evaporation. The circular metal electrodes had diameters of either 100 μm or 50 μm and were separated by a gap of 15 μm from a concentric contact, as shown in Figure 2.

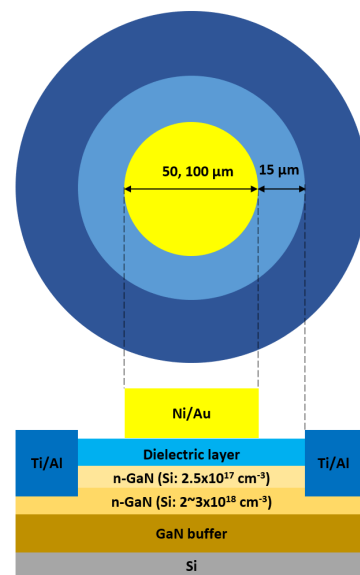


Figure 2. Cross-sectional schematic of the fabricated metal-insulator-semiconductor (MIS) capacitors.

XRD and XRR measurements were performed using a SmartLab diffractometer (Rigaku, Tokyo, Japan) to determine the crystallinity and mass density of the AlN film, respectively. The cross-sections at the AlN/GaN interface were examined using a STEM (JEM-2100F, JEOL). The chemical bonding states and components of AlN were determined via XPS (SIGMA PROBE, ThermoFisher Scientific, Waltham, MA, USA). Time-of-flight (TOF)-SIMS (TOF-SIMS.5, ION-TOF, Münster, Germany) analysis was also performed on the AlN film to investigate the presence of GaO_x at the AlN/GaN interface.

The J–E_{eff} and C–V characteristics of AlN/AlON/AlHfON on GaN MIS capacitors were also investigated. An AlON/AlHfON layer was deposited onto the AlN layer to reduce the leakage current and increase the dielectric constant. AlON/AlHfON on GaN MIS capacitors were also fabricated as reference devices. The effective electric field was defined as (applied voltage–flat band voltage)/capacitance-equivalent thickness (CET). PEALD AlON, and AlHfON films were deposited using trimethylaluminum (TMA), tetrakis(dimethylamido)hafnium (TDMAHf), N₂ plasma, and ozone as the Al, Hf, N, and O precursors, respectively. The substrate temperature and N₂ plasma power were 330 °C and 30 W, respectively. The AlHfON film was deposited using the nanolaminate technique with alternating stacks of AlON and HfO₂ films with an equal cycle ratio of 1:1.

3. Results

Figure 3 shows the growth rate per cycle (GPC) as a function of the process step time. The deposition temperature was 330 °C, and the NH₃ plasma power was 100 W. The GPC was saturated at a TMA feeding time of 0.1 s and NH₃ plasma time of 10 s, and the saturated value was 1.1 Å/cycle. The purge times after the TMA precursor injection and NH₃ plasma step were chosen as 7 and 10 s, respectively.

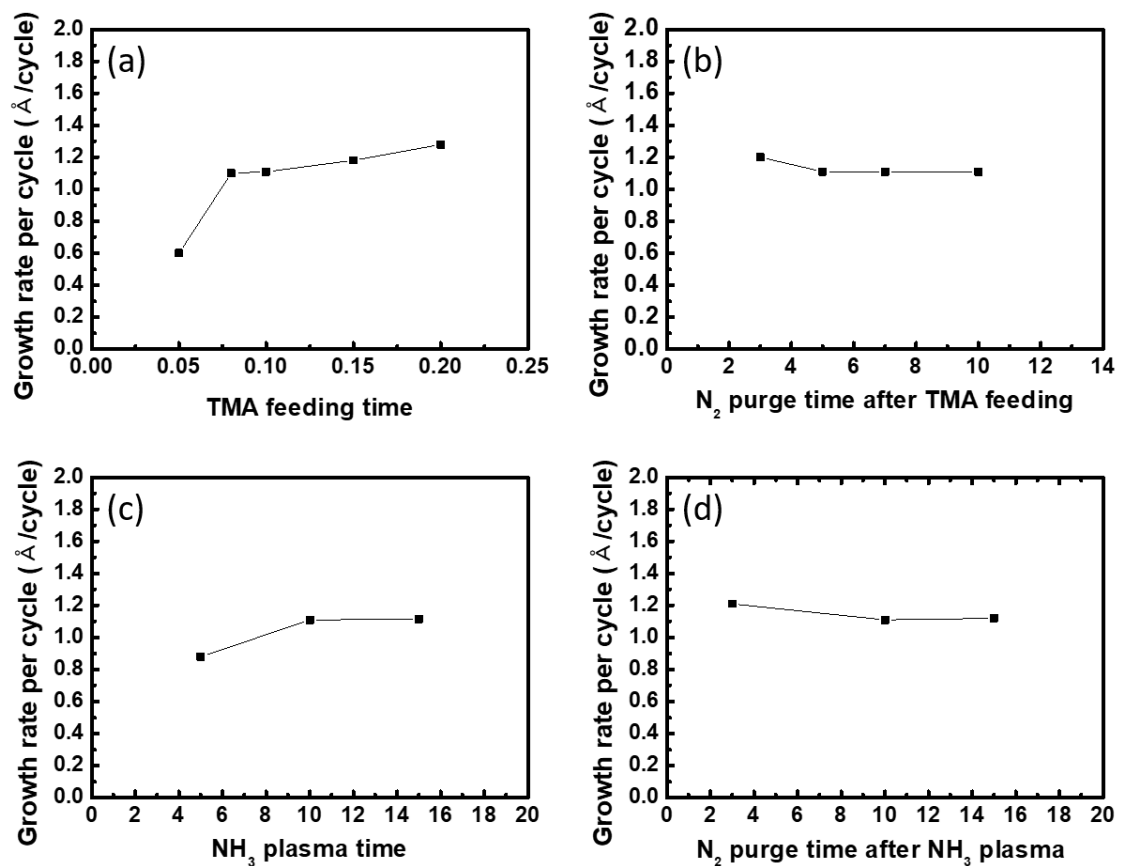


Figure 3. (a–d) Growth rate per cycle (GPC) values for AlN deposited using the PEALD system as a function of the trimethylaluminum (TMA) feeding time, N₂ purge time after TMA feeding, NH₃ plasma time, and N₂ purge time after NH₃ plasma (NH₃ plasma power: 100 W).

Figure 4 shows the linear dependence of the AlN film thickness, measured using ellipsometry, on the number of ALD cycles. The thickness increased linearly as the number of cycles increased without any incubation period. An interface layer was not observed between the Si and AlN, which can be attributed to the suppression of surface oxidation by AlN.

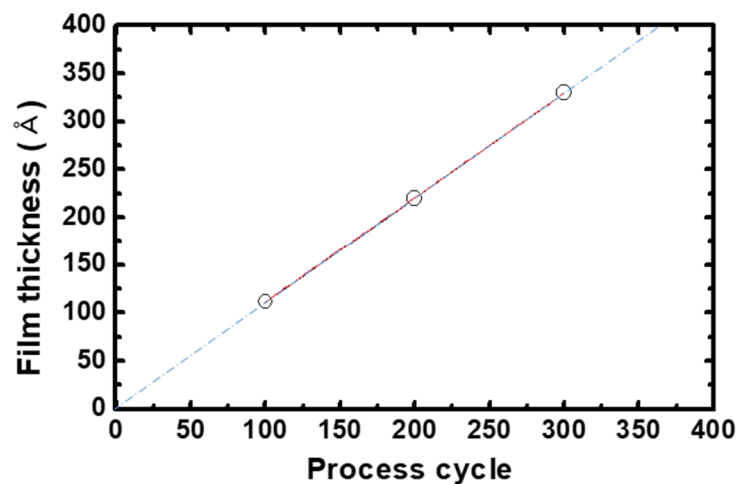


Figure 4. AlN film thickness values as a function of ALD cycles (NH₃ plasma power: 100 W).

Figure 5 shows the double sweep C–V characteristics of AlN on n-GaN capacitors with various NH₃ plasma powers when the bias was swept from –5 V to 2 V and back to –5 V.

The C–V measurements were performed at 1 MHz. The C–V hysteresis characteristics of the MIS capacitors were almost identical regardless of the change in the NH₃ plasma power, and exhibited minor hysteresis. The dielectric constants of the AlN films prepared using 30, 50, and 100 W NH₃ plasma were 8.2, 7.8, and 8.1, respectively.

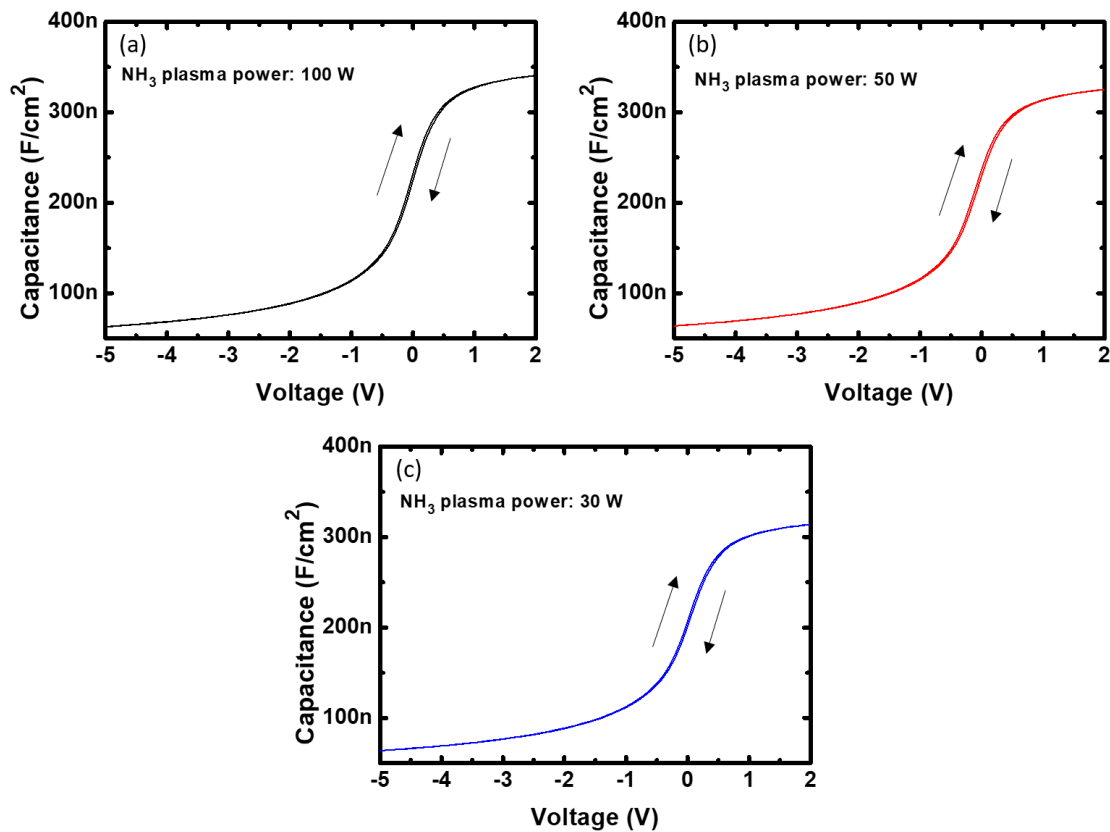


Figure 5. C–V characteristics of the AlN metal-insulator-semiconductor (MIS) capacitors. NH₃ plasma power (AlN thickness): (a) 100 W (20.8 nm), (b) 50 W (21.3 nm), and (c) 30 W (22.9 nm).

The J–E characteristics of AlN on the n-GaN capacitor with an NH₃ plasma power of 30 W indicated a higher breakdown field and lower leakage current at a low electrical field compared to the other capacitors with plasma powers over 30 W, as shown in Figure 6. The low plasma power at the NH₃ plasma step was considered to reduce the plasma-induced damage on the n-GaN surface, resulting in better J–V characteristics of the AlN on the n-GaN capacitor [28]. In conclusion, a TMA feeding time of 0.1 s, purge time of 7 s after the TMA precursor injection step, NH₃ gas stabilization time of 3 s, NH₃ plasma time of 10 s at 30 W, purge time of 10 s after the NH₃ plasma step, and deposition temperature of 330 °C were chosen as the optimized deposition conditions for the fabrication of AlN on n-GaN.

To investigate the film quality, various characterization methods were conducted using films deposited under optimum conditions. Figure 7a shows the θ – 2θ XRD patterns of a 100 nm-thick AlN layer deposited on n-GaN. Two diffraction peaks at 2θ values of $\sim 33^\circ$, and $\sim 36^\circ$ were observed, which corresponded to the (100) and (002) planes, respectively [29,30]. The peak at $\sim 31^\circ$ is an artifact related to the high power of 9 kW. As shown in Figure 7b, the crystal quality was characterized using the rocking curve of AlN (002). The measured full width at half-maximum (FWHM) was 1050 arcsec, and the density of the ALD AlN which was evaluated by fitting the XRR data was 3.27 g/cm³, which is higher than the values reported in earlier studies [31,32]. These results indicate that highly crystalline AlN can be achieved at a low growth temperature of 330 °C.

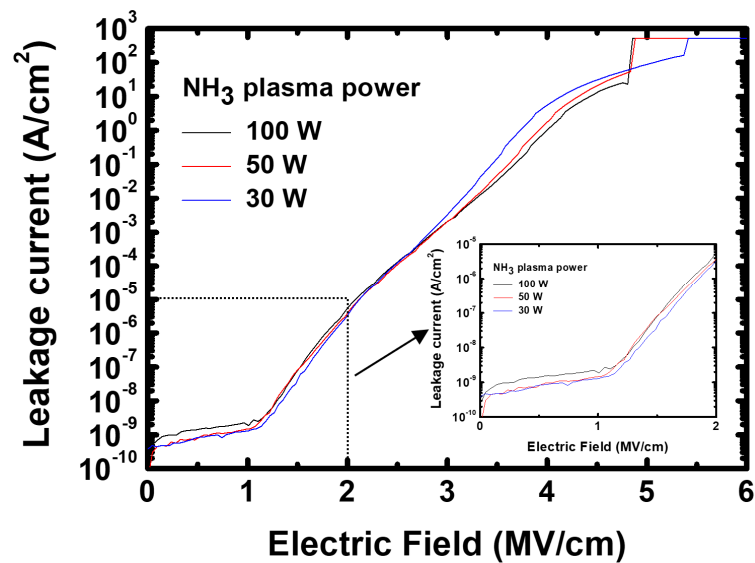


Figure 6. J–E characteristics of the MIS capacitors.

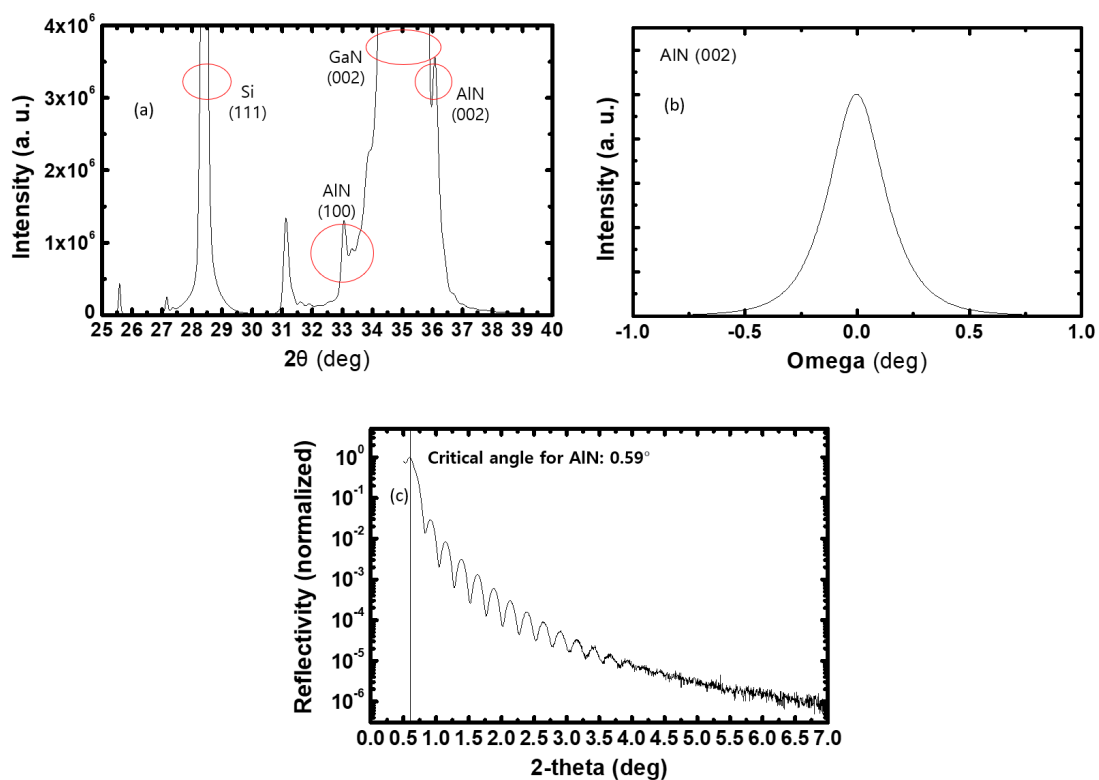


Figure 7. (a) XRD result and (b) rocking curve of (002) of the ALD AIN of ~100 nm on n-GaN and (c) XRR result of the ALD AIN of ~30 nm on n-GaN (NH_3 plasma power: 30 W).

Figure 8 shows the STEM cross-sectional image of ~10 nm AIN on n-GaN. Crystalline AIN was observed in the image, and a sharp interface between the n-GaN and ALD AIN was confirmed, indicating the successful suppression of the surface oxidation of GaN by the introduction of an AIN layer.

Figure 9 shows the XPS spectra of Al2p, N1s, C1s, and O1s of ~22 nm AIN on n-GaN. The deconvoluted Al2p spectra show two peaks at binding energies of 73.6 eV and 74.2 eV, which are associated with Al–N and Al–O bonds, respectively [33]. Binding energies of 396.5 eV and 398.4 eV were observed in the deconvoluted N1s spectra and are associated

with N–Al and N–O–Al bonds, respectively [33]. The atomic concentrations of Al, N, C, and O in AlN were 47.4%, 44.2%, 0.9%, and 7.5%, respectively.

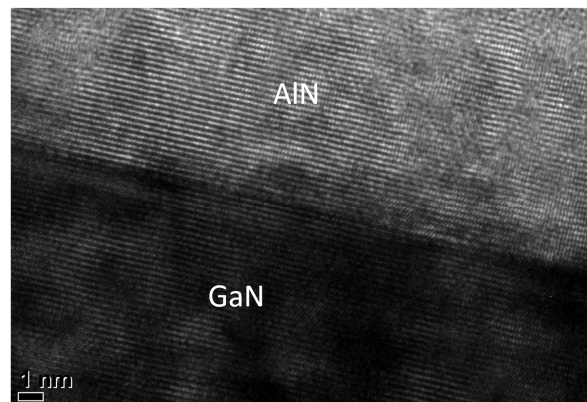


Figure 8. Cross-sectional STEM image of the AlN/n-GaN interface (NH_3 plasma power: 30 W).

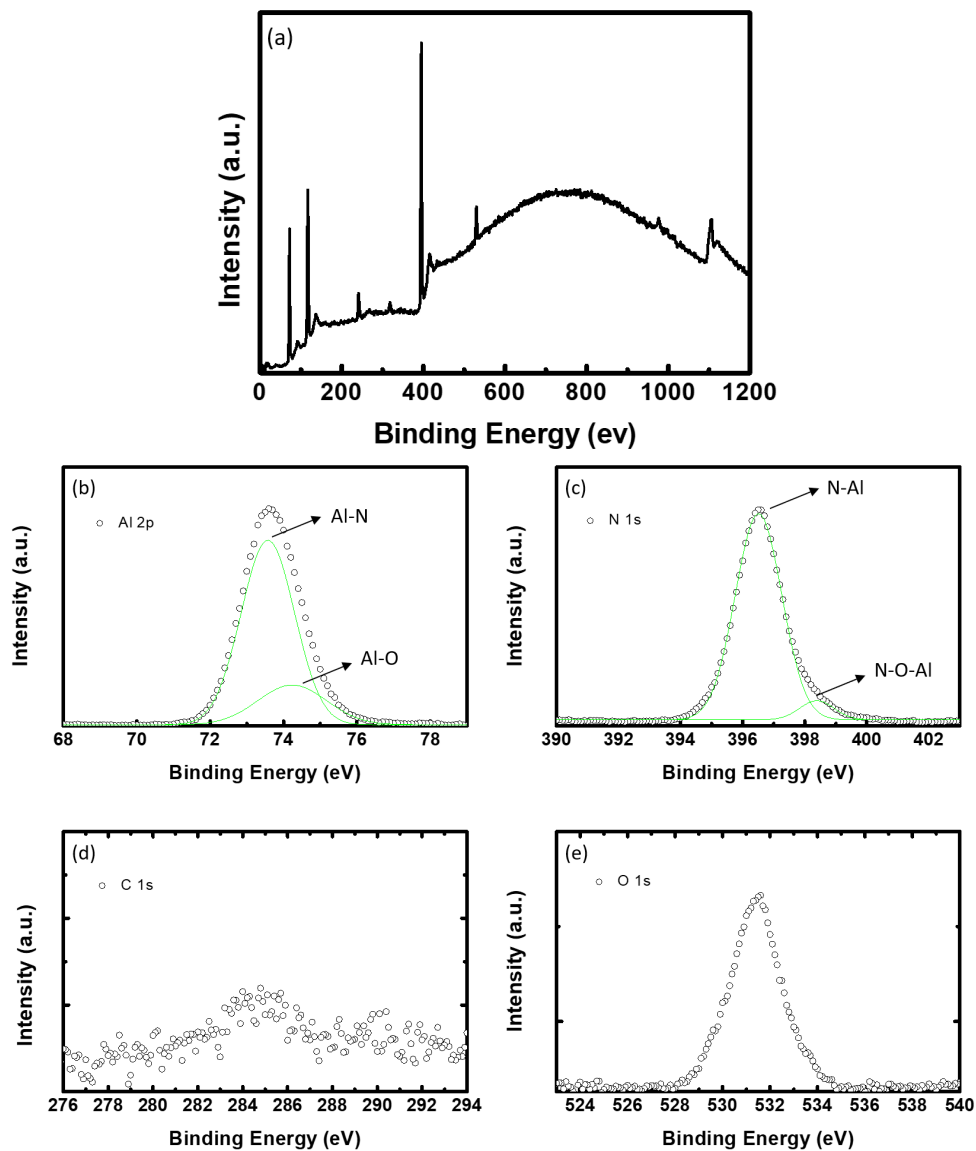


Figure 9. (a) Wide-scan XPS spectra and high-resolution XPS spectra of the (b) Al 2p, (c) N 1s, (d) C 1s, and (e) O 1s of the ALD AlN (NH_3 plasma power: 30 W).

As previously discussed, the AlN layer showed low C–V hysteresis, confirming that it efficiently suppressed charge injection into the dielectrics. A low breakdown field of ~ 5 MV/cm and a high leakage current for an applied electric field of 2 MV/cm were also observed in the AlN MIS capacitors. An AlON/AlHfON layer was employed on the AlN layer to increase the breakdown field and reduce the leakage current of AlN. TOF-SIMS analysis of AlON/AlHfON and AlN/AlON/AlHfON on the n-GaN layer was conducted to obtain further information about the interface between AlN and n-GaN, and the results are shown in Figure 10. The oxygen intensity at the AlON/n-GaN interface was higher than that at the AlN/n-GaN interface, whereas the gallium intensity slope observed at the AlN/n-GaN interface was steeper than that observed at the AlON/n-GaN interface. These observations imply that using ALD AlN as an interfacial layer has an advantage compared to the use of AlON with O_3 oxidant at the III–V interface because ALD AlN suppresses surface oxidation.

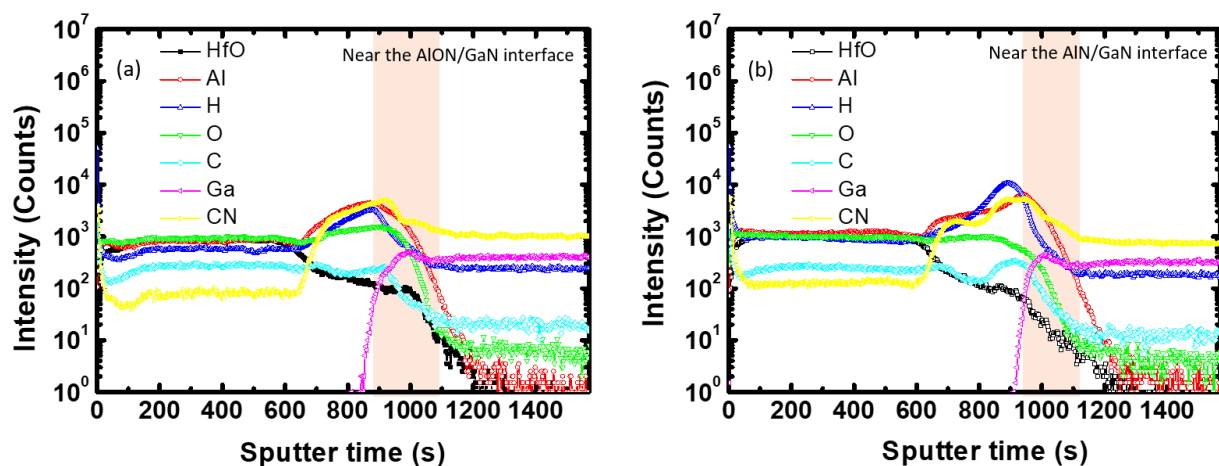


Figure 10. Time-of-flight (TOF)-secondary ion mass spectrometry (SIMS) results for (a) AlON/AlHfON ($\sim 5/\sim 15$ nm) and (b) AlN/AlON/AlHfON ($\sim 2/\sim 3/\sim 15$ nm) on n-GaN (NH_3 plasma power: 30 W).

To evaluate the immunity against electron injection into the dielectrics, repeated C–V measurements were performed by sweeping the applied voltage from the accumulation to the depletion region [14]. The maximum accumulation voltage was increased in steps of 1 V by 5 V, and the depletion voltage was set to -10 V. The C–V characteristics of the MIS capacitors swept from the accumulation to depletion region, and the V_{FB} shift of MIS capacitors as a function of the accumulation voltage are shown in Figure 11a–c. The MIS capacitor with AlN as an interfacial layer exhibited a smaller V_{FB} shift compared to the MIS capacitor without the AlN interfacial layer. A V_{FB} drift of 242 mV was observed for the MIS capacitor with AlN after sweeping from 5 V to -10 V, whereas a V_{FB} drift of 365 mV was confirmed for the MIS capacitor without AlN. This difference indicates that there are fewer interface states between AlN and GaN than between AlON and GaN owing to the suppression of the formation of interfacial oxides. Figure 11d shows the $J-E_{eff}$ characteristics of the fabricated MIS capacitors. Despite the high leakage current characteristics of AlN, the MIS capacitor with AlN as an interfacial layer exhibited leakage current characteristics similar to those of MIS capacitors without AlN.

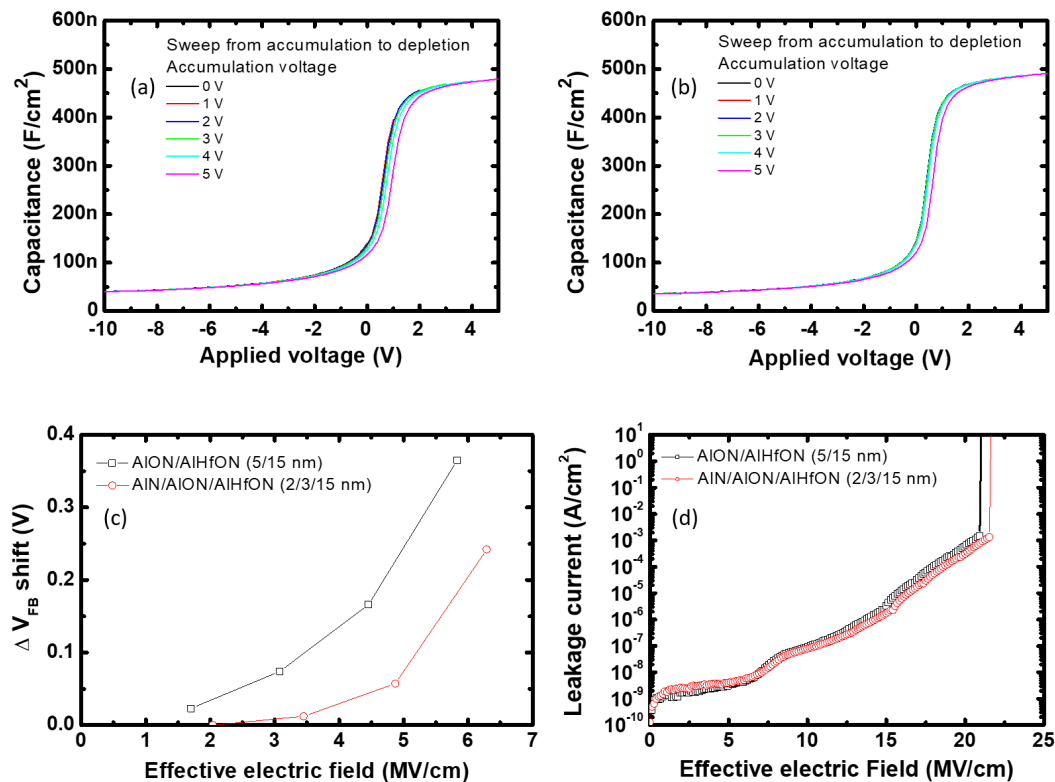


Figure 11. (a,b) C–V characteristics of the GaN MIS capacitors with accumulation voltages ranging from 0 V to 5 V; (c) V_{FB} shift as a function of the effective electric field in the fabricated GaN MIS capacitors; and (d) J – E_{eff} characteristics of the fabricated MIS capacitors (NH_3 plasma power: 30 W).

4. Conclusions

An AlN interfacial layer using TMA and NH_3 plasma in a PEALD system was developed to improve the dielectric/GaN interface characteristics. The optimized AlN process conditions were as follows: TMA feeding for 0.1 s, N_2 purge for 7 s after TMA feeding, NH_3 gas stabilization for 3 s, NH_3 plasma for 10 s at 30 W, N_2 purge for 10 s after NH_3 plasma, and a deposition temperature of 330 °C. The PEALD process ensured a high linearity between the AlN thickness and the number of cycles. Two different diffraction peaks at 2θ values of $\sim 33^\circ$ and $\sim 36^\circ$ corresponding to (100) and (002) planes, respectively, were observed in the XRD measurements, and the density of the ALD AlN was 3.27 g/cm³ from the XRR measurement. The AlN interfacial layer successfully suppressed the GaN surface oxidation and improved the V_{FB} drift characteristics of the MIS capacitor, showing excellent leakage current characteristics. Thus, it is suggested that the low-temperature PEALD AlN is a promising interfacial layer with a high crystal quality for GaN.

Author Contributions: Process set-up: I.-H.H. and M.-J.K.; investigation: I.-H.H. and M.-J.K.; formal analysis: I.-H.H.; conceptualization: I.-H.H., H.-Y.C., and K.-S.S.; methodology: I.-H.H., H.-Y.C., and K.-S.S.; visualization: I.-H.H.; writing—original draft preparation: I.-H.H., H.-Y.C., and K.-S.S.; writing—review and editing: I.-H.H., H.-Y.C., and K.-S.S.; supervision: H.-Y.C. and K.-S.S. All authors have read and agreed to the published version of the manuscript.

Funding: This work was supported by the Ministry of Trade, Industry & Energy (10067636) and the Basic Science Research Program (No. 2015R1A6A1A03031833 and No. 2019R1A2C1008894).

Acknowledgments: Myoung-Jin Kang currently works at the future technology R&D center, SK Hynix Co., Ltd., KOREA.

Conflicts of Interest: The authors declare no conflict of interest.

References

1. Lu, Y.; Yang, S.; Jiang, Q.; Tang, Z.; Li, B.; Chen, K.J. Characterization of V_T -instability in enhancement-mode Al_2O_3 -AlGaIn/GaN MIS-HEMTs. *Phys. Status Solidi Curr. Top. Solid State Phys.* **2013**, *10*, 1397–1400. [\[CrossRef\]](#)
2. Lagger, P.; Ostermaier, C.; Pobegen, G.; Pogany, D. Towards understanding the origin of threshold voltage instability of AlGaIn/GaN MIS-HEMTs. *Tech. Dig. Int. Electron Devices Meet. IEDM* **2012**, 299–302. [\[CrossRef\]](#)
3. He, J.; Hua, M.; Zhang, Z.; Chen, K.J. Performance and V_{TH} Stability in E-Mode GaN Fully Recessed MIS-FETs and Partially Recessed MIS-HEMTs with LPCVD-SiN_x/PECVD-SiN_x Gate Dielectric Stack. *IEEE Trans. Electron Devices* **2018**, *65*, 3185–3191. [\[CrossRef\]](#)
4. Wada, Y.; Nozaki, M.; Hosoi, T.; Shimura, T.; Watanabe, H. Insight into gate dielectric reliability and stability of SiO_2 /GaN MOS devices. *Jpn. J. Appl. Phys.* **2020**, *59*. [\[CrossRef\]](#)
5. Lee, J.G.; Kim, H.S.; Seo, K.S.; Cho, C.H.; Cha, H.Y. High quality PECVD SiO_2 process for recessed MOS-gate of AlGaIn/GaN-on-Si metal-oxide-semiconductor heterostructure field-effect transistors. *Solid State Electron.* **2016**, *122*, 32–36. [\[CrossRef\]](#)
6. Hu, Q.; Li, S.; Li, T.; Wang, X.; Li, X.; Wu, Y. Channel engineering of normally-OFF AlGaIn/GaN MOS-HEMTs by atomic layer etching and high- κ Dielectric. *IEEE Electron Device Lett.* **2018**, *39*, 1377–1380. [\[CrossRef\]](#)
7. Maeda, E.; Nabatame, T.; Yuge, K.; Hirose, M.; Inoue, M.; Ohi, A.; Ikeda, N.; Shiozaki, K.; Kiyono, H. Change of characteristics of n-GaN MOS capacitors with Hf-rich HfSiO_x gate dielectrics by post-deposition annealing. *Microelectron. Eng.* **2019**, *216*, 111036. [\[CrossRef\]](#)
8. Hwang, I.H.; Eom, S.K.; Choi, G.H.; Kang, M.J.; Lee, J.G.; Cha, H.Y.; Seo, K.S. High-Performance E-Mode AlGaIn/GaN MIS-HEMT with Dual Gate Insulator Employing SiON and HfON. *Phys. Status Solidi Appl. Mater. Sci.* **2018**, *215*, 1–6. [\[CrossRef\]](#)
9. Kim, H.S.; Han, S.W.; Jang, W.H.; Cho, C.H.; Seo, K.S.; Oh, J.; Cha, H.Y. Normally-Off GaN-on-Si MISFET Using PECVD SiON Gate Dielectric. *IEEE Electron Device Lett.* **2017**, *38*, 1090–1093. [\[CrossRef\]](#)
10. Jiang, H.; Tang, C.W.; Lau, K.M. Enhancement-Mode GaN MOS-HEMTs with Recess-Free Barrier Engineering and High- κ ZrO₂ Gate Dielectric. *IEEE Electron Device Lett.* **2018**, *39*, 405–408. [\[CrossRef\]](#)
11. Anderson, T.J.; Wheeler, V.D.; Shahin, D.I.; Tadjer, M.J.; Koehler, A.D.; Hobart, K.D.; Christou, A.; Kub, F.J.; Eddy, C.R. Enhancement mode AlGaIn/GaN MOS high-electron-mobility transistors with ZrO₂ gate dielectric deposited by atomic layer deposition. *Appl. Phys. Express* **2016**, *9*, 071003. [\[CrossRef\]](#)
12. Uenuma, M.; Takahashi, K.; Sonehara, S.; Tominaga, Y.; Fujimoto, Y.; Ishikawa, Y.; Uenuma, M.; Takahashi, K.; Sonehara, S.; Tominaga, Y. Influence of carbon impurities and oxygen vacancies in Al_2O_3 film on Al_2O_3 /GaN MOS capacitor characteristics. *AIP Adv.* **2018**, 105103. [\[CrossRef\]](#)
13. Zhu, J.; Hou, B.; Chen, L.; Zhu, Q.; Yang, L.; Zhou, X.; Zhang, P.; Ma, X.; Hao, Y. Threshold Voltage Shift and Interface/Border Trapping Mechanism in Al_2O_3 /AlGaIn/GaN MOS-HEMTs. In Proceedings of the 2018 IEEE International Reliability Physics Symposium (IRPS), Burlingame, CA, USA, 11–15 March 2018; pp. 8–11. [\[CrossRef\]](#)
14. Nozaki, M.; Watanabe, K.; Yamada, T.; Shih, H.A.; Nakazawa, S.; Anda, Y.; Ueda, T.; Yoshigoe, A.; Hosoi, T.; Shimura, T.; et al. Implementation of atomic layer deposition-based AlON gate dielectrics in AlGaIn/GaN MOS structure and its physical and electrical properties. *Jpn. J. Appl. Phys.* **2018**, *57*, 06KA02. [\[CrossRef\]](#)
15. Kang, M.J.; Eom, S.K.; Kim, H.S.; Lee, C.H.; Cha, H.Y.; Seo, K.S. Normally-off recessed-gate AlGaIn/GaN MOS-HFETs with plasma enhanced atomic layer deposited AlO_xN_y gate insulator. *Semicond. Sci. Technol.* **2019**, *34*. [\[CrossRef\]](#)
16. Liu, C.; Chor, E.F.; Tan, L.S. Enhanced device performance of AlGaIn/GaN HEMTs using HfO₂ high- κ dielectric for surface passivation and gate oxide. *Semicond. Sci. Technol.* **2007**, *22*, 522–527. [\[CrossRef\]](#)
17. Chang, Y.C.; Huang, M.L.; Chang, Y.H.; Lee, Y.J.; Chiu, H.C.; Kwo, J.; Hong, M. Atomic-layer-deposited Al_2O_3 and HfO₂ on GaN: A comparative study on interfaces and electrical characteristics. *Microelectron. Eng.* **2011**, *88*, 1207–1210. [\[CrossRef\]](#)
18. Ozaki, S.; Ohki, T.; Kanamura, M.; Imada, T.; Nakamura, N.; Okamoto, N.; Miyajima, T.; Kikkawa, T. Effect of oxidant source on threshold voltage shift of AlGaIn/GaN MIS-HEMTs using ALD- Al_2O_3 gate insulator films. In Proceedings of the 2012 CS MANTECH Conference, Boston, MA, USA, 23–26 April 2012; pp. 3–6.
19. Yang, S.; Tang, Z.; Wong, K.; Lin, Y.; Liu, C.; Lu, Y.; Huang, S.; Chen, K.J. High-Quality Interface in Al_2O_3 /GaN/GaNAlGaInGaN MIS Structures with in Situ Pre-Gate Plasma Nitridation. *IEEE Electron Device Lett.* **2013**, *34*, 1497–1499. [\[CrossRef\]](#)
20. Shen, Z.; He, L.; Zhou, G.; Yao, Y.; Yang, F.; Ni, Y.; Zheng, Y.; Zhou, D.; Ao, J.; Zhang, B.; et al. Investigation of O_3 - Al_2O_3 /H₂O- Al_2O_3 dielectric bilayer deposited by atomic-layer deposition for GaN MOS capacitors. *Phys. Status Solidi Appl. Mater. Sci.* **2016**, *213*, 2693–2698. [\[CrossRef\]](#)
21. Eom, S.K.; Kong, M.W.; Kang, M.J.; Lee, J.G.; Cha, H.Y.; Seo, K.S. Enhanced Interface Characteristics of PA-ALD HfO_xN_y/InGaAs MOSCAPs Using IPA Oxygen Reactant and Cyclic N₂ Plasma. *IEEE Electron Device Lett.* **2018**, *39*, 1636–1639. [\[CrossRef\]](#)
22. Huang, S.; Jiang, Q.; Yang, S.; Zhou, C.; Chen, K.J. Effective passivation of AlGaIn/GaN HEMTs by ALD-grown AlN thin film. *IEEE Electron Device Lett.* **2012**, *33*, 516–518. [\[CrossRef\]](#)
23. Hsieh, T.E.; Chang, E.Y.; Song, Y.Z.; Lin, Y.C.; Wang, H.C.; Liu, S.C.; Salahuddin, S.; Hu, C.C. Gate recessed quasi-normally off Al_2O_3 /AlGaIn/GaN MIS-HEMT with low threshold voltage hysteresis using PEALD AlN interfacial passivation layer. *IEEE Electron Device Lett.* **2014**, *35*, 732–734. [\[CrossRef\]](#)
24. Kim, H.; Kim, N.D.; An, S.C.; Yoon, H.J.; Choi, B.J. Improved interfacial properties of thermal atomic layer deposited AlN on GaN. *Vacuum* **2019**, *159*, 379–381. [\[CrossRef\]](#)

25. Tarala, V.A.; Altakhov, A.S.; Martens, V.Y.; Lisitsyn, S.V. Growing aluminum nitride films by Plasma-Enhanced Atomic Layer Deposition at low temperatures. In *Journal of Physics: Conference Series*; IOP Publishing: Bristol, UK, 2015; p. 652. [[CrossRef](#)]
26. Dallaeva, D.S.; Bilalov, B.A.; Gitikchiev, M.A.; Kardashova, G.D.; Safaraliev, G.K.; Tománek, P.; Škarvada, P.; Smith, S. Structural properties of Al₂O₃/AlN thin film prepared by magnetron sputtering of Al in HF-activated nitrogen plasma. *Thin Solid Films* **2012**, *526*, 92–96. [[CrossRef](#)]
27. Dallaev, R.; Sobola, D.; Tofel, P.; Škvarenina, L.; Sedlák, P. Aluminum nitride nanofilms by atomic layer deposition using alternative precursors hydrazinium chloride and triisobutylaluminum. *Coatings* **2020**, *10*, 954. [[CrossRef](#)]
28. Knoops, H.C.M.; Faraz, T.; Arts, K.; Kessels, W.M.M. (Erwin) Status and prospects of plasma-assisted atomic layer deposition. *J. Vac. Sci. Technol. A* **2019**, *37*, 030902. [[CrossRef](#)]
29. Shih, H.Y.; Lee, W.H.; Kao, W.C.; Chuang, Y.C.; Lin, R.M.; Lin, H.C.; Shiojiri, M.; Chen, M.J. Low-temperature atomic layer epitaxy of AlN ultrathin films by layer-by-layer, in-situ atomic layer annealing. *Sci. Rep.* **2017**, *7*, 1–8. [[CrossRef](#)]
30. Zhu, Z.; Ostreng, E.; Tuoriniemi, I.; Chen, Z.; Niiranen, K.; Sneck, S. Batch atomic layer deposition of aluminum nitride for RF-MEMS and GAN power-devices. In Proceedings of the 2019 China Semiconductor Technology International Conference (CSTIC), Shanghai, China, 18–19 March 2019; pp. 1–3. [[CrossRef](#)]
31. Abdulagatov, A.I.; Ramazanov, S.M.; Dallaev, R.S.; Murliev, E.K.; Palchaev, D.K.; Rabadanov, M.K.; Abdulagatov, I.M. Atomic Layer Deposition of Aluminum Nitride Using Tris(diethylamido)aluminum and Hydrazine or Ammonia. *Russ. Microelectron.* **2018**, *47*, 118–130. [[CrossRef](#)]
32. Alevli, M.; Ozgit, C.; Donmez, I.; Biyikli, N. Structural properties of AlN films deposited by plasma-enhanced atomic layer deposition at different growth temperatures. *Phys. Status Solidi Appl. Mater. Sci.* **2012**, *209*, 266–271. [[CrossRef](#)]
33. Cao, D.; Cheng, X.; Xie, Y.H.; Zheng, L.; Wang, Z.; Yu, X.; Wang, J.; Shen, D.; Yu, Y. Effects of rapid thermal annealing on the properties of AlN films deposited by PEALD on AlGa_{0.5}N/GaN heterostructures. *RSC Adv.* **2015**, *5*, 37881–37886. [[CrossRef](#)]